

# **ANALYSIS AND COMPARISON OF DIFFERENT MODELING APPROACHES FOR THE SIMULATION OF A MICRO-SCALE ORGANIC RANKINE CYCLE POWER PLANT**

Rémi Dickes\*, Olivier Dumont, Arnaud Legros, Sylvain Quoilin, Vincent Lemort

Energy System Research Unit  
Aerospace and Mechanical Engineering Department  
Faculty of Applied Sciences  
University of Liège  
Belgium

\* Corresponding Author (rdickes@ulg.ac.be)

## **ABSTRACT**

When simulating a system based on the organic Rankine cycle (ORC), different modeling methods can be used to predict its performance. Each method is characterized by advantages, limitations and a level of complexity. This contribution aims to assess the impact of the modeling approach on the performance prediction of ORC systems. To this end, a 2.8 kWe ORC unit is investigated as case study. In this paper, the components of the test bench are modeled using different approaches of increasing complexity and each model is calibrated using experimental data from the test rig. The goodness of fit as well as the benefits and limitations of each modeling methods are analyzed and discussed.

## **1. INTRODUCTION**

Because of the depletion of fossil fuels and global warming issues, the world of energy is undergoing many changes toward increased sustainability. Among the different technologies in development, power plant based on the organic Rankine cycle (ORC) are playing a key role in low-grade temperature applications such as waste heat recovery (Quoilin et al., 2011), geothermal power (DiPippo, 2004) or solar thermal energy (Georges et al., 2013). An organic Rankine cycle is a thermal power system used for the conversion of heat into mechanical work by means of the thermodynamic Rankine cycle. Its working principle and its components are similar to a conventional steam power plant but it uses an organic refrigerant as working fluid instead of water.

As for many other technologies, modeling and simulation of ORC systems is crucial for design, sizing or control purposes. From single polynomial correlations predicting the global power plant efficiency to detailed deterministic simulations of each component, several modeling approaches of different complexity levels can be used to predict the performance of an ORC. Each method has its advantages and limitations, and the most appropriate approach for one application is not necessarily the same for another. The objective of this work is to assess the impact of the modeling complexity on the performance prediction of ORC systems. To this end, a 2.8 kWe ORC unit is investigated as case study (Dickes et al., 2014). The test bench uses R245fa as working fluid and consists of a scroll expander, an air-cooled condenser, a gear pump, a recuperator and an oil-heated evaporator. In this paper, each component of the power plant is simulated with three different modeling methods and each model is calibrated using experimental data from the test rig. The goodness of fit as well as the benefits and limitations of the different modeling approaches are discussed. The following sections focus respectively on the pump, the evaporator, the condenser and the expander.

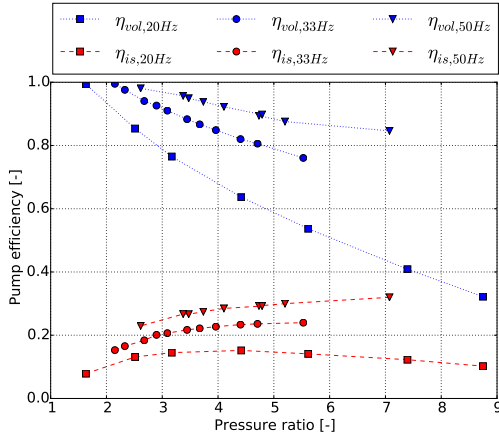


**Figure 1: Experimental efficiencies of the gear pump in function of the shaft speed and pressure ratio**

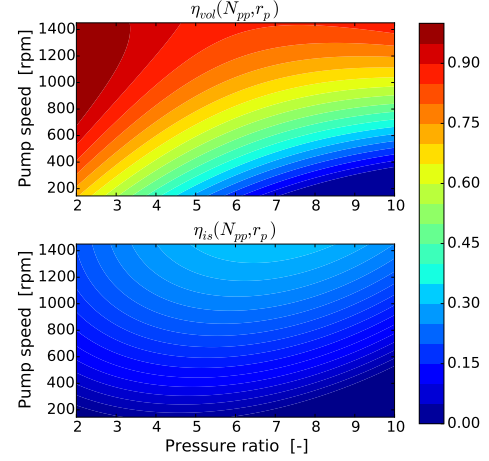


**Figure 2: Second-order polynomial correlations modeling the pump isentropic and volumetric efficiencies**

## 2. PUMP

The device used to pressurize the working fluid in the ORC test bench is a gear pump (model: Viking *SG-80550-MOV*). As shown in Figure 1, experimental measurements on the test rig demonstrate a significant influence of the pressure ratio and of the shaft speed on the pump performance (i.e. its isentropic efficiency  $\eta_{is,pp}$  and its volumetric efficiency  $\eta_{vol,pp}$ ). In order to predict the mechanical power consumption and the mass flow rate delivered by the pump, three different modeling approaches are investigated.

### 2.1 Constant-efficiency model (method PP<sub>A</sub>)

A simple method to simulate a pump is to neglect the effect of the operating conditions on the machine performance. Such assumption allows to model the pump with constant volumetric and isentropic efficiencies i.e.

$$\eta_{is,pp} = \frac{\dot{m}_{pp}(h_{ex,is,pp} - h_{su,pp})}{\dot{W}_{mec,pp}} = \bar{\eta}_{is,pp} \quad \eta_{vol,pp} = \frac{\dot{V}_{su,pp}}{N_{pp}V_{dis,pp}} = \bar{\eta}_{vol,pp} \quad (1)$$

where  $\dot{m}_{pp}$  and  $\dot{V}_{su,pp}$  are respectively the fluid mass and volumetric flow rates,  $\dot{W}_{mec,pp}$  is the pump mechanical power,  $N_{pp}$  is the pump rotation speed and  $V_{dis,pp}$  is the machine displacement volume. Based on experimental measurements or manufacturer data, the calibration of the two parameters  $\bar{\eta}_{vol,pp}$  and  $\bar{\eta}_{is,pp}$  is straightforward and can be performed with a single operating point. If data for several operating conditions are available, an average value of each efficiency is generally selected.

### 2.2 Physically-based model (method PP<sub>B</sub>)

Alternatively, the pump can be simulated using a semi-empirical model (also referred to as lumped parameter model) which implements physically-based equations. In this work, the effective mass flow delivered by the pump  $\dot{m}_{pp}$  is calculated as an ideal mass flow rate  $\dot{m}_{ideal,pp}$  to which an internal recirculation flow rate  $\dot{m}_{lk,pp}$  is deduced. The mass flow rate characterizing the internal leakages is modeled by means of an incompressible flow through an equivalent orifice as suggested by Declaye (2015):

$$\dot{m}_{pp} = \underbrace{(\rho_{su,pp} N_{pp} V_{s,pp})}_{\dot{m}_{ideal,pp}} - \underbrace{(A_{lk} \sqrt{2\rho_{su}(P_{pp,ex} - P_{pp,su})})}_{\dot{m}_{lk,pp}} \quad (2)$$

where  $P_{pp,ex}$  and  $P_{pp,su}$  are respectively the pressures at the inlet and the exhaust of the pump,  $\rho_{su,pp}$  is the inlet density of the fluid and  $A_{leak}$  is the surface area of the equivalent orifice. The mechanical consumption of the pump is calculated by adding mechanical losses  $\dot{W}_{loss,pp}$  to the isentropic power  $\dot{W}_{is,pp}$ . These mechanical losses are calculated by means of constant losses  $\dot{W}_0$  added to a term proportional to the isentropic power i.e.

$$\dot{W}_{mec,pp} = \underbrace{(\dot{W}_0 + K_0 \dot{V}_{su,pp}(P_{pp,ex} - P_{pp,su}))}_{\dot{W}_{loss,pp}} + \underbrace{(\dot{V}_{su,pp}(P_{pp,ex} - P_{pp,su}))}_{\dot{W}_{is,pp}} \quad (3)$$

Based on the identification of three parameters, namely  $A_{leak}$ ,  $K_0$  and  $\dot{W}_0$ , the model can extrapolate the machine behavior while accounting for the influence of the operating conditions on the pump performance. The calibration of the parameters is performed by minimizing the deviation between the reference data and the simulation results. A minimum of two different operating points is required to identify the three parameters but the higher the number of data, the better the calibration.

### 2.3 Polynomial model (method PP<sub>C</sub>)

Finally, a second-order polynomial correlation can be tuned to predict the pump efficiency as depicted in Figure 2. Such empirical model fits correctly the experimental data and provides good predictions of interpolated behaviors. However, extrapolations of the performance outside of the calibration range is unadvised. Indeed, the polynomial expressions could provide unrealistic values of  $\eta_{is,pp}$  and  $\eta_{vol,pp}$ . The number of data points should also be high to avoid effects such as overfitting or the Runge's phenomenon. In this work, a second-order polynomial equation in function of the pressure ratio and the pump speed has been identified to best fit the experimental efficiencies of the pump:

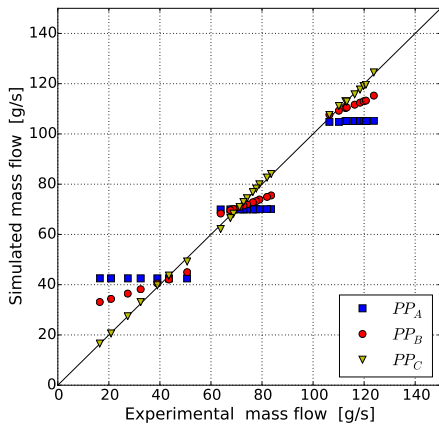
$$\eta_{is,pp} = \sum_{i=0}^2 \sum_{j=0}^2 a_{ij} r_p^i N_{pp}^j \quad \eta_{vol,pp} = \sum_{k=0}^2 \sum_{l=0}^2 b_{kl} r_p^k N_{pp}^l \quad (4)$$

### 2.4 Comparison of the results

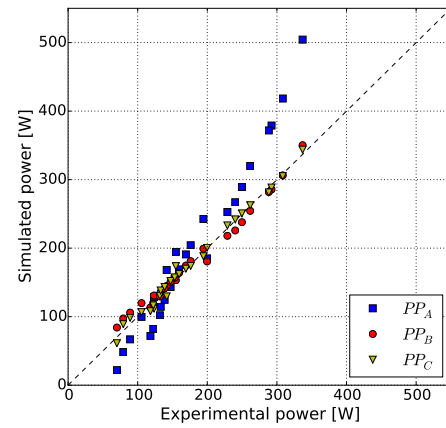
The three models PP<sub>A</sub>, PP<sub>B</sub> and PP<sub>C</sub> are calibrated using an experimental database of 27 operating points. Detailed values of the parameters are given in the Appendix and the coefficients of determination  $R^2$  resulting of the calibration are summarized in Table 1. The deviation between simulation results and experimental data is also illustrated in Figure 3. The basic constant-efficiency model (method PP<sub>A</sub>) leads to the largest fitting residues and a maximum relative error of 160% and 69% is committed for the mass flow rate and for the mechanical power respectively. The second-order polynomial correlations demonstrate the best fit but they are characterized by severe modeling restrictions as discussed in section 2.3. The semi-empirical model PP<sub>B</sub> which implements physically-based equations appears to be the best compromise between model complexity (only 3 parameters to be identified), goodness of fit and performance extrapolation. Although the mechanical power consumption is correctly reproduced, an alternative formulation of the recirculation losses should be investigated to improve the prediction of the pump mass flow rate.

## 3. EVAPORATOR AND CONDENSER

The evaporator and the condenser installed in the ORC test bench are respectively a counterflow brazed heat exchanger (model: Alfa Laval CB76-100E) and an air-cooled fin coil heat exchanger (model: Alfa Laval Solar Junior-121). Although the condenser presents a multipass crossflow arrangement, the number of passes for each tube in the air flow is considered high enough ( $N_{pass} = 4$ ) to simulate the heat transfer as a counterflow configuration (Shah and Sekulic, 2003). For both the evaporator and the condenser, a single component performs the heat transfer resulting in the co-existence of three refrigerant phases inside the heat exchangers. In the case of the evaporator (resp. the condenser), the total surface area is divided in three zones (see Figure 4), namely the preheating (resp. the subcooling) zone, the vaporization (resp. the condensation) zone and the superheating (resp. the de-superheating) zone. In this



(a) Predicted mass flow rate vs. experimental data



(b) Predicted power vs. experimental data

**Figure 3: Goodness of fit of the pump models PP<sub>A</sub>, PP<sub>B</sub> and PP<sub>C</sub>**

work, three different modeling methods are investigated to predict the performance of the evaporator and the condenser.

### 3.1 Constant-pinch model (method HEX<sub>A</sub>)

A simple method to model a three-zone heat exchanger is to impose a constant pinch between the temperature profiles of the cold and the hot fluid. As depicted in Figure 5, the pinch  $\theta$  can be located differently along the temperature profiles in function of the operating conditions and the type of heat exchanger (condenser or evaporator). In a general statement, one can formulate the constant-pinch paradigm as follows:

$$\min(\Delta T_c; \Delta T_l; \Delta T_v; \Delta T_h) = \bar{\theta} \quad \text{with} \quad \begin{cases} \Delta T_c = |T_{htf,c} - T_{wf,c}| \\ \Delta T_l = |T_{htf,l} - T_{wf,l}| \\ \Delta T_v = |T_{htf,v} - T_{wf,v}| \\ \Delta T_h = |T_{htf,h} - T_{wf,h}| \end{cases} \quad (5)$$

where the temperatures of the heat transfer fluid  $T_{htf,i}$  and the working fluid  $T_{wf,i}$  are referred as depicted in Figure 5. The calibration of the unique parameter  $\bar{\theta}$  is straightforward and it can be performed using experimental results of a single point. If data in several operating conditions are available, a mean value of the pinch is chosen. The model is easily implemented but the assumption of a constant pinch over a wide range of conditions can lead to significant errors in the performance evaluation of an heat exchanger.

### 3.2 Three-zone model with constant heat transfer coefficients (method HEX<sub>B</sub>)

Another approach to simulate the evaporator and the condenser is to decompose the modeling into the different zones of the heat exchanger. Each zone is characterized by a global heat transfer coefficient  $U_i$  and a heat transfer surface area  $A_i$ . The global heat transfer coefficient is evaluated by considering only two convective heat transfer resistances in series whereas the surface area is computed using the logarithm mean temperature difference method. In the case of the evaporator, both fluids have the same heat transfer surface area and  $A_i$  is evaluated in each zone as follows:

$$U_i = \left( \frac{1}{\alpha_{wf,i}} + \frac{1}{\alpha_{htf,i}} \right)^{-1} \quad A_i = \frac{\dot{Q}_i}{U_i \Delta T_{log,i}} \quad (6)$$

where  $\alpha_{wf,i}$  and  $\alpha_{htf,i}$  are the convective heat transfer coefficients of the two fluids,  $\dot{Q}_i$  is the heat power transferred in each zone and  $\Delta T_{log,i}$  is the related logarithm mean temperature difference. In the case of

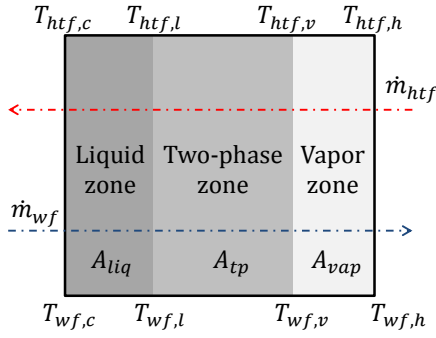


**Figure 4: Three-zone moving-boundary model of an evaporator**

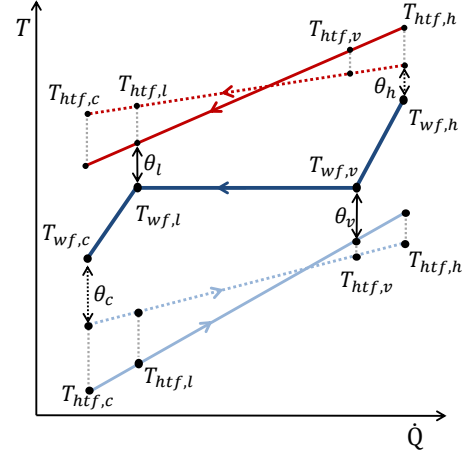


**Figure 5: Pinch locations in a three-zone heat exchanger**

the air-cooled condenser, the heat transfer surface area is not the same for the two fluids since it is a fin coil heat exchanger. For each zone, the surface area on the refrigerant side  $A_{wf,i}$  is evaluated i.e.

$$U_i^* = \left( \frac{1}{\alpha_{wf,i}} + \frac{1}{\eta_{s,i}(A_{htf}/A_{wf})\alpha_{htf,i}} \right)^{-1} \quad A_{wf,i} = \frac{\dot{Q}_i}{U_i^* \Delta T_{log,i}} \quad (7)$$

where  $\eta_{s,i}$  is the overall air-side surface efficiency and  $A_{htf}/A_{wf}$  is the ratio between the heat transfer surface areas of the two fluids. The efficiency  $\eta_{s,i}$  is defined by Incropera and Witt (1996) as

$$\eta_{s,i} = 1 - \frac{A_{fin}}{A_{htf}}(1 - \eta_{fin,i}) \quad (8)$$

where  $A_{fin}$  is the fins area,  $A_{htf}$  is the total air-side heat transfer area and  $\eta_{fin,i}$  is the fin efficiency. The calculation of the fin efficiency is performed using the Schmidt method. For the sack of conciseness, the set of equations leading to  $\eta_{fin,i}$  is not provided in this paper. For any further information, refer to Stewart (2003) which provides a complete description of the modeling method. The temperature profiles inside the heat exchanger correspond to the situation in which the total surface area simulated by model is equal to the geometrical surface area of the component  $A_{hex}$ , i.e.

$$A_{hex} = A_{liq} + A_{tp} + A_{vap} \quad (9)$$

In this second modeling method, the convective heat transfer coefficients are assumed constant whatever the operating conditions. For the refrigerant, different values are assigned for each zone whereas a single coefficient characterizes the secondary fluid. Therefore, the semi-empirical model relies on four parameters:  $\alpha_{wf,liq}$ ,  $\alpha_{wf,tp}$ ,  $\alpha_{wf,vap}$  and  $\alpha_{htf}$ . The calibration of these parameters is not difficult if the reference database includes operating conditions with a unique zone on the refrigerant side (i.e. operating conditions with only a liquid phase, a vapor phase or two-phase in the refrigerant flow). In such conditions, the surface area of the zone is known ( $A_{liq|tp|vap} = A_{hex}$ ) and the heat transfer coefficients can be identified easily. However, if the database used for the calibration consists of experimental points with multi-zone operating conditions, the calibration process becomes more challenging since the surface area dedicated to each zone is unknown. To identify the heat transfer coefficients, an optimization process must be performed over the complete database to minimize an error function. In this work, the temperature profiles are provided as inputs and the coefficients are optimized in order to minimize the global error committed on the surface area i.e.

$$\min \sum_{j=1}^M \frac{1}{M} \left| \frac{A_{hex} - A_{liq,j} - A_{tp,j} - A_{vap,j}}{A_{hex}} \right| \quad (10)$$

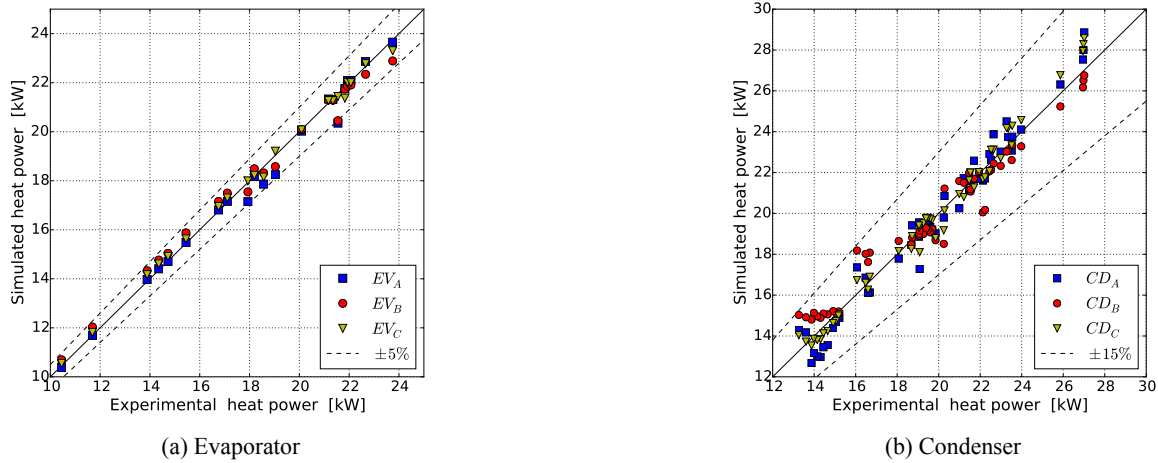


Figure 6: Predicted vs. experimental heat power transferred in the heat exchangers

### 3.3 Three-zone model with variable heat transfer coefficients (method $HEX_C$ )

The third modeling approach investigated in this work is based on the same model paradigm of method  $HEX_B$ . However, instead of keeping the convective heat transfer coefficients constant in all operating conditions, it is proposed to account for the effect of the mass flow rate on the heat transfer by means of the following relations (Quoilin et al., 2008)

$$\alpha_{wf,i} = \alpha_{wf,n,i} \left( \frac{\dot{m}_{wf}}{\dot{m}_{wf,n}} \right)^{0.8} \quad \alpha_{hff} = \alpha_{hff,n} \left( \frac{\dot{m}_{hff}}{\dot{m}_{hff,n}} \right)^{0.8} \quad (11)$$

where  $\alpha_{wf,n,i}$  and  $\alpha_{hff,n}$  are parameters illustrating the heat transfer coefficients of the fluids in case of nominal mass flow rates ( $\dot{m}_{wf,n}$  and  $\dot{m}_{hff,n}$ ). Like for the second modeling approach, each zone on the refrigerant side is characterized by different coefficients whereas a single nominal heat transfer coefficient  $\alpha_{hff,n}$  is assigned for the secondary fluid. Four parameters must be identified and the calibration procedure has the same characteristics as discussed in section 3.2.

### 3.4 Comparison of the results

The three modeling methods are applied for both the condenser and the evaporator. The models are calibrated using experimental data from the test bench and the deviations between simulation results and experimental data are illustrated in Figure 6. Detailed values of the parameters are available in the Appendix and the coefficient of determination  $R^2$  are summarized in Table 1. The constant-pinch model (method  $HEX_A$ ) is the simplest method to implement and to calibrate. Since the operating points used for the calibration are with a relatively constant pinch, this modeling method demonstrates the second best fit to experimental data eventhough a single parameter is required. However, the ability of such modeling approach is limited for performance extrapolations over a wide range of operating conditions as explained in section 3.1. The three-zone moving-boundary model with constant heat transfer coefficients (method  $HEX_B$ ) presents opposite characteristics. Its calibration is more complex and requires the use of an optimization process. Although it shows the lowest goodness of fit, the consideration of each zone in the heat exchanger makes it more reliable for performance extrapolation in different operating conditions. Finally, by accounting for the impact of the mass flow rate on the heat transfer, the method  $HEX_C$  demonstrates the best fit and the best ability for performance extrapolation. However, its calibration is as complex as for method  $HEX_B$  since it also requires an optimization process.

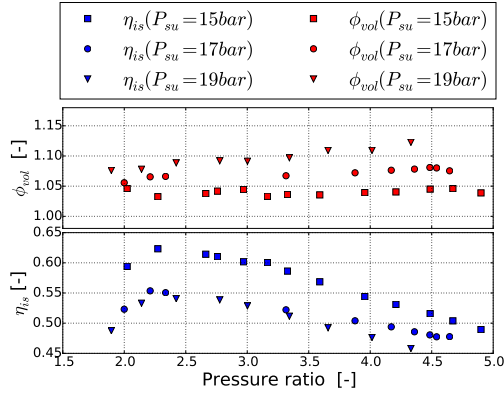


**Figure 7: Isentropic efficiency and filling factor of the expander**

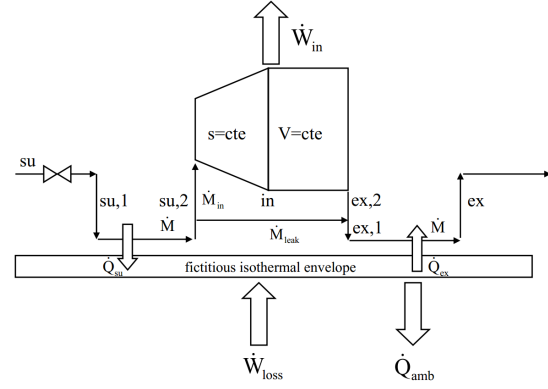


**Figure 8: Semi-empirical model of the scroll expander (Lemort, 2008)**

## 4. EXPANDER

The expansion process is performed by a scroll compressor modified to run in reverse as an expander (model: Copeland ZR34 K3E-ZD). It is directly connected to the grid and its shaft speed remains constant in any situation. As depicted in Figure 7, experimental measurements demonstrate an influence of the pressure ratio and the fluid supply conditions on the machine performance (i.e. the isentropic efficiency  $\eta_{is,exp}$  and the filling factor  $\phi_{vol,exp}$  (Quoilin, 2011)). In this contribution, three modeling methods are investigated to extrapolate the expander behavior in different operating conditions.

### 4.1 Constant-efficiency model (method EXP<sub>A</sub>)

Similarly to the pump, the simplest method to simulate an expander is to assume a constant performance whatever the operating conditions. In such case, the isentropic efficiency  $\bar{\eta}_{is,exp}$  and the filling factor  $\bar{\phi}_{vol,exp}$  of the machine are identified and set constant as explained in section 2.1. However, the temperature range in an expander is higher than in a pump resulting in unnegligible heat losses if the expander is not thermally insulated. In order to account for the effect of these losses on the exhaust conditions, a third parameter  $AU_{loss}$  can be added to the model i.e.:

$$\dot{m}_{exp} (h_{su,exp} - h_{ex,exp}) = \dot{W}_{mec,exp} + AU_{loss} (\bar{T}_{exp} - T_{amb}) \quad (12)$$

### 4.2 Physically-based model (method EXP<sub>B</sub>)

The second approach chosen for simulating the expander performance is the physically-based model proposed by Lemort (2008). The conceptual scheme of the model is shown in Figure 8 and a complete description of the governing equations can be found in Lemort et al. (2009). Besides of under- and over-expansion losses due to the fixed built-in volumetric ratio of the machine, the model accounts for internal leakages, mechanical losses, pressure drops at the inlet and heat losses. Unlike deterministic modeling methods which require the exact knowledge of the machine geometry (Dickes, 2013), the semi-empirical model can extrapolate the expander performance in a wide range of operating conditions by the identification of eight parameters. The calibration of the parameters is not direct and must be performed through an optimization process minimizing the global error committed on the model outputs (Lemort et al., 2009).

### 4.3 Polynomial correlations (method EXP<sub>C</sub>)

A third modeling approach is to evaluate the expander performance by means of a second-order polynomial correlation. As discussed in section 2.3, these models are suitable to interpolate the machine behavior within the calibration range but extrapolations of the performance outside of this confidence domain is unadvised. In this work, a second-order polynomial equation in function of the supply density

**Table 1: Goodness of fit for the different models**  
 (\* : if heat losses are modeled in the expander)

Pump model	$R^2[\dot{m}_{pp}]$	$R^2[\dot{W}_{pp,mec}]$	$R^2[\dot{W}_{pp,elec}]$
PP <sub>A</sub>	0.788	0.805	0.802
PP <sub>B</sub>	0.951	0.981	0.982
PP <sub>C</sub>	0.999	0.991	0.991
Evaporator model	$R^2[\dot{Q}_{ev}]$	$R^2[T_{wf,ex}]$	$R^2[T_{hf,ex}]$
EV <sub>A</sub>	0.9995	0.9314	0.9043
EV <sub>B</sub>	0.9994	0.7942	0.999
EV <sub>C</sub>	0.9998	0.9479	0.9995
Condenser model	$R^2[\dot{Q}_{cd}]$	$R^2[T_{wf,ex}]$	$R^2[T_{hf,ex}]$
CD <sub>A</sub>	0.968	0.748	0.987
CD <sub>B</sub>	0.932	0.118	0.985
CD <sub>C</sub>	0.981	0.86	0.996
Expander model	$R^2[\dot{m}_{exp}]$	$R^2[\dot{W}_{exp,mec}]$	$R^2[T_{wf,ex}]$
EXP <sub>A</sub>	0.9826	0.9621	0.3695/0.9309*
EXP <sub>B</sub>	0.9768	0.9848	0.8626
EXP <sub>C</sub>	0.996	0.9906	0.3783/0.9151*

( $\rho_{su}$ ) and the logarithm of pressure ratio ( $\ln(r_p)$ ) is used to characterize the isentropic efficiency and filling factor of the expander i.e.

$$\eta_{is,exp} = \sum_{i=0}^2 \sum_{j=0}^2 a_{ij} (\ln(r_p))^i \rho_{su}^j \quad \phi_{vol,exp} = \sum_{k=0}^2 \sum_{l=0}^2 b_{kl} (\ln(r_p))^k \rho_{su}^l \quad (13)$$

Similarly to method EXP<sub>A</sub>, heat losses can be taken into account by using equation (12).

#### 4.4 Comparison of the results

The three modeling methods EXP<sub>A</sub>, EXP<sub>B</sub> and EXP<sub>C</sub> are calibrated using an experimental database of 53 operating points. The coefficients of determination  $R^2$  from the calibration are summarized in Table 1 and detailed values of the parameters are provided in the Appendix. The constant-efficiency model permits a good fit of the experimental results if heat losses are taken into account, but significant errors are committed on the exhaust temperature otherwise. Since a constant efficiency is assigned to the machine performance while experimental measurements demonstrate an influence of the operating conditions, significant errors can be committed while extrapolating the machine performance out of the calibration range. In contrast to method EXP<sub>A</sub>, the polynomial model accounts for the influence of the operating conditions on the expander performance and fits the best the experimental data. However, such correlation presents severe modeling restrictions as discussed in section 4.3 and it is more sensitive to the dataset used for the calibration. The semi-empirical model EXP<sub>B</sub> overcomes these issues. By implementing physically-based equations, extrapolation of the expander performance can be performed out of the confidence range and the model calibration is less sensitive to the experimental points used as reference. However, the identification of the eight parameters is not as straightforward as for the two other methods since it requires a non-linear optimization process as explained in section 4.3.

## 5. CONCLUSION AND FUTURE WORK

The performance evaluation of an ORC system can be carried out using different modeling methods. In order to assess the impact, the advantages and the limitations of different approaches, a 2.8 kWe ORC unit is investigated as reference case. Each component of the micro-scale power plant is simulated by



**Table 2: Characteristics of the different models**  
 (\* : if heat losses are modeled in the expander)

	PP <sub>A</sub>	PP <sub>B</sub>	PP <sub>C</sub>	HEX <sub>A</sub>	HEX <sub>B</sub>	HEX <sub>C</sub>	EXP <sub>A</sub>	EXP <sub>B</sub>	EXP <sub>C</sub>
Nbr. of parameters	2	3	8	1	4	4	2/3*	8	8/9*
Goodness of fit	-	+	+	≈	-	+	-/≈*	+	-/+*
Simplicity of calibration	+	≈	≈	+	-	-	+	-	+
Performance extrapolation	≈	+	-	-	≈	+	-/≈*	+	-
	+ : good			≈ : neutral			- : bad		

means of three modeling methods characterized by different levels of complexity. All the models are calibrated with experimental data from the test rig and a comparison is performed in terms of goodness of fit and calibration complexity. A deeper investigation about extrapolation capability will be performed by means of a cross validation process and by comparing the models prediction with other experimental datasets. The main observations of the current analysis are summarized in Table 2. In this paper, the components are considered alone. Future works will apply a similar analysis to the model of the whole system by interconnecting the models of each subcomponent. The global behavior of the test rig will be evaluated over a wide range of operating conditions and deviations between the different modeling approaches will be analyzed.

## NOMENCLATURE

### Symbols

$A$	surface area ( $m^2$ )
$a, b$	polynomial coefficients (-)
$\Delta T$	temperature difference ( $K$ )
$h$	specific enthalpy ( $J/kg$ )
$\dot{m}$	mass flow ( $kg/s$ )
$N$	shaft speed ( $rpm$ )
$P$	pressure ( $Pa$ )
$\dot{Q}$	heat power ( $W$ )
$r_p$	pressure ratio (-)
$T$	temperature ( $K$ )
$U$	global heat coefficient ( $W/m^2.K$ )
$V$	volume ( $m^3$ )
$\dot{V}$	volumetric flow ( $m^3/s$ )
$\dot{W}$	Power ( $W$ )
$\alpha$	convective heat coefficient ( $W/m^2.K$ )
$\eta$	efficiency (-)
$\varphi$	filling factor (-)
$\rho$	density ( $kg/m^3$ )
$\theta$	pinch ( $K$ )

### Subscripts

amb	ambiance
c	cold
cd	condenser
dis	displacement
ex	exhaust
exp	expander
ev	evaporator
h	hot
hex	heat exchanger
htf	heat transfer fluid
is	isentropic
l, liq	liquid
lk	leakage
log	logarithm
mec	mecanichal
n	nominal
pp	pump
su	supply
tp	two-phase
v, vap	vapor
vol	volumetric
wf	working fluid

## APPENDIX

The appendices include detailed values of the parameters for each model presented in this paper and additional Figures illustrating the deviations between simulation results and experimental data. The appendix is available in electronic form only at the following url: <http://hdl.handle.net/2268/180069>

## REFERENCES

- Declaye, S. (2015). *Improving the performance of micro-ORC systems*. PhD thesis, University of Liège.
- Dickes, R. (2013). Design and fabrication of a variable wall thickness two-stage scroll expander to be integrated in a micro-solar power plant. Master's thesis, University of Liège.
- Dickes, R., Dumont, O., Declaye, S., Quoilin, S., Bell, I., and Lemort, V. (2014). Experimental investigation of an orc system for a micro-solar power plant. In *Proceedings of the 22<sup>nd</sup> International Compressor Engineering Conference at Purdue*.
- DiPippo, R. (2004). Second law assessment of binary plants generating power from low-temperature geothermal fluids. *Geothermics*, 33:565--586.
- Georges, E., Declaye, S., Dumont, O., Quoilin, S., and Lemort, V. (2013). Design of a small-scale orc engine used in a solar power plant. *Internation Journal of Low-Carbon Technologies*.
- Incropera, F. and Witt, D. D. (1996). *Fundamentals of Heat and Mass Transfer*. John Wiley and Sons, Inc.
- Lemort, V. (2008). *Contribution to the characterization of scroll machines in compressor and expander modes*. PhD thesis, University of Liège.
- Lemort, V., Quoilin, S., Cuevas, C., and Lebrun, J. (2009). Testing and modeling a scroll expander integrated into an organic rankine cycle. *Applied Thermal Engineering*, 29:3094--3102.
- Quoilin, S. (2011). *Sustainable energy conversion through the use of organic Rankine cycles for waste heat recovery and solar applications*. PhD thesis, University of Liège.
- Quoilin, S., Aumann, R., Grill, A., Schuster, A., Lemort, V., and Spliethoff, H. (2011). Dynamic modeling and optimal control strategy of waste heat recovery. *Applied Energy*, 88:2183--2190.
- Quoilin, S., Orosz, M. S., and Lemort, V. (2008). Modeling and experimental investigation of an organic rankine cycle using scroll expander for small scale solar applications. In *Proceedings of the 1st Eurosun Conference*.
- Shah, R. and Sekulic, D. (2003). *Fundamentals of Heat Exchanger Design*. John Wiley and Sons, Inc.
- Stewart, S. W. (2003). *Enhanced finned-tube condenser design and optimization*. PhD thesis, Georgia Institute of Technology.